The Anisotropy of Dimensional Change on Sintering of Iron

Alberto Molinari*, Elisa Torresani*, Cinzia Menapace*, and Mats Larsson**

*D epartment of Industrial Engineering, University of Trento, Trento, Italy

** Höganäs AB, SE-263 83 Höganäs, Sweden

Abstract

The anisotropy of dimensional change on the sintering of iron was investigated by dilatometry. Dimensional changes are different along the longitudinal and transversal directions, and shrinkage is more pronounced parallel to the compaction direction. This phenomenon is particularly pronounced during the early stage of sintering, in the alpha field below the Curie temperature. The results were elaborated according to the kinetics model for shrinkage to calculate an effective diffusion coefficient along the two directions. Such an effective diffusion coefficient is higher parallel to the compaction direction than perpendicular to it, and both are larger than the diffusion coefficient calculated on the basis of the activation energy reported in the literature for pure iron. This discrepancy is attributed to the defectiveness introduced by cold compaction in the particle contact regions, which may enhance diffusivity owing to the dislocation pipe mechanism, which, in turn, is particularly intense below the Curie temperature. This interpretation may also justify anisotropy of shrinkage because the powder particles are inhomogeneously deformed by uniaxial cold compaction. The enhanced diffusion coefficient increases with time and shows a maximum at temperatures below the Curie point. This trend was discussed with reference to the self-activated sintering mechanism.

I. Introduction

Sintering shrinkage of uniaxially cold compacted iron and iron alloys is anisotropic. The most common behaviour results in a larger shrinkage along the compaction direction than in the compaction plane,[1-3] and the presence of a liquid phase by Cu and P addition reduces shrinkage anisotropy.[3] In swelling systems, expansion in the compaction plane is larger than that along the compaction direction. [4,5] Anisotropy of dimensional change is the subject of a theoretical analysis by several authors using continuum mechanics that correlate anisotropy to pore morphology,[6] particle rearrangement,[7–9] and gravity.[10] A contribution to anisotropy may also result from the application of a nonisotropic strain or stress field to the sintering body (constrained sintering).[11] Zavaliangos et al.[12,13] proposed additional phenomena responsible for anisotropy: elongated particles, gas pore pressure, interface porosity, and crystallographic texture, as well as other structural and geometrical features of prior cold compacted green bodies such as the different flattening and orientation of interparticle contacts and a different “quality” of the grain boundary between particles in terms of interface pores and oxide fragmentation promoted by prior compaction. Most of the theoretical works do not consider that metal powder particles are plastically deformed by cold compaction and are thus highly strain hardened. This structural condition of the powder particles is expected to affect mass transport phenomena responsible for shrinkage. A systematic study of the shrinkage kinetics of prior uniaxially cold compacted ferrous materials was conducted by performing dilatometry tests on specimens cut along the

directions parallel (longitudinal) and perpendicular (transversal) to the compaction direction. In case of a cold isostatically pressed iron green compact, dilatometry curves of specimens cut along different directions do not show significant differences, confirming the expected isotropic shrinkage.[14,15] Conversely, a noticeable difference is displayed by the curves of uniaxially cold compacted iron alloys, particularly in the early stage of sintering in the alpha field below the Curie transformation [1,16,17]: the longitudinal specimen starts shrinking at a lower temperature than the transversal specimen. The same behavior was observed in Cr–Mo low-alloy steel at higher temperatures in the austenitic region.[18] By means of dilatometry, it was also possible to recognize the contribution of the liquid phase in Fe–Cu and Fe–P alloys; owing to the uneven packing of the green body, liquid phase spreads inhomogeneously among the solid particles, enhancing the transversal shrinkage over the longitudinal shrinkage, thus attenuating anisotropy with respect to pure iron.19 To highlight the phenomena responsible for anisotropy of dimensional change, isothermal sintering experiments were performed in the temperature ranges at which a pronounced anisotropy was observed. Isothermal shrinkage curves were then elaborated with reference to the shrinkage kinetic model proposed by the sintering theory based on the rigid spheres model, and the following results were obtained[15,18]:

1. The main mass transport mechanism responsible for shrinkage is volume diffusion, with a diffusion coefficient much higher than that calculated from the activation energy for pure iron;
2. The diffusion coefficient depends on temperature and the isothermal sintering time; it increases with time and in some cases reaches a maximum and then decreases;
3. The time-dependent diffusion coefficient is higher in the longitudinal direction than in the transversal direction. These results were interpreted by considering plastic deformation caused by cold compaction, which promotes the accumulation of dislocations in the contact regions.

Dislocations enhance volume diffusion through the pipe dislocation diffusion mechanism.[20] When the diffusion distance is much higher than the mean separation between dislocations, the diffusion depth is greater than it would be without dislocations, and an effective diffusivity directly proportional to the dislocation density is defined. Shima et al.[21] demonstrated that the pipe diffusivity is up to six orders of magnitude higher than the volume diffusion coefficient of iron in the temperature range 600°C–800°C. This may justify the strongly enhanced shrinkage below the Curie point in iron and, considering the inhomogeneous distribution of plastic deformation of the powder particles after uniaxial cold compaction, its anisotropy. The role of dislocations in sintering and shrinkage kinetics was proposed by Friedrich and Schatt,[22–25] who investigated the evolution of the structure of lattice defects (dislocations and vacancy agglomerates) in the contact regions during sintering of pure Ni and Cu. In addition to dislocations formed during cold compaction, vacancies are produced by the transformation of the high-energy contact (cold weld joint) to the high-angle grain boundary with a lower energy. These agglomerates may transform at high temperatures in dislocations, which, according to their theory, activates shrinkage by dislocation creep (self-activated sintering mechanism). These authors defined an effective diffusion coefficient proportional to the dislocation density and may be up to two orders of magnitude larger than the diffusion coefficient in the presence of an equilibrium density of dislocations. An even larger increase in the diffusion coefficient was

reported by Lanyi and Hermel,[26] who introduced the concept of structural activity to describe the contribution to shrinkage of lattice defects not in equilibrium. Because the previous works on iron alloys featured experiments that were performed below the Curie transformation, in this study, the investigation was extended to the whole temperature range between 640°C and 1120°C to investigate the differences in the shrinkage kinetics between the longitudinal and transversal directions above the Curie temperature and in the austenite field up to the common sintering temperature of industrial production. The isothermal shrinkage curves were elaborated with reference to the classical theory of sintering, calculating the effective diffusion coefficients along the two directions. Results were discussed with reference to the hypothesized evolution with temperature and time of structural defects introduced by cold compaction and formed during sintering.

II. Experimental Procedure

An atomized iron powder (25% of particles <45 μm) was mixed with 0.6 wt% amide wax as a lubricant. Charpy impact bars (55 mm x 10 mm x 10 mm) were uniaxially cold compacted up to a 6.9 g/cm^3 green density and deluded at 550°C for one hour in argon. Prismatic specimens (10 mm x 3 mm x 3 mm) were cut both parallel and perpendicular to the compaction direction (longitudinal and transversal specimens in the following, respectively) for the dilatometry experiments. A Baehr dilatometer equipped with induction heating was used, and a thermocouple for temperature control was welded to the specimen. The atmosphere in the dilatometer chamber was a vacuum at 5 x 10^{-4} mbar. Experiments were performed at various temperatures from 640°C to 1120°C, with a 0.5°C/s heating rate and 3600 s isothermal holding.

III. Results and Discussion

Figure 1 shows the dilatometric record of the longitudinal and transversal specimens during the test at 1060°C.

Fig. 1. Dilatometry curves up to 1060°C for the longitudinal and transversal specimens

During the heating step, a deviation from the linear expansion is observed at approximately 630°C, indicating the start of shrinkage, followed by a maximum in the curve and a net contraction up to the Curie temperature. Above T_C, the slope is still smaller than that at the beginning of the test, indicating a continuous contribution of shrinkage to dimensional change. These phenomena are more pronounced in the longitudinal specimen than in the transversal specimen, whereas the slope of the curves relevant to the two specimens above the alpha/gamma transformation and during the isothermal holding is rather similar. These results confirm what was observed in the previous works[1,16]: shrinkage starts at low temperatures with a significant anisotropy in the ferritic region, and particularly below the Curie point; in the austenitic region, both during heating and the isothermal holding, anisotropy of dimensional change is much less pronounced. Figure 2 shows the isothermal shrinkage curves of the two specimens at 680°C, 815°C, and 1060°C, as representative of the other curves in the three temperature ranges mentioned above: below the Curie point, in the alpha field above T_C, and in the austenite field.

Fig. 2. Examples of isothermal shrinkage curves at T < Tc, Tc < T < Tα/γ, and T > Tα/γ.

The difference in the isothermal shrinkage between the longitudinal and transversal specimens is much higher below T_C ($\Delta l/l_{0,long}/\Delta l/l_{0,trans}$ = 2 at 680°C) than at the other two temperatures (1.2 and 1.4 at 815°C and 1060°C, respectively). Moreover, below the Curie point, the slopes of the curves sharply change after approximately 400 s (transversal) and 700 s (longitudinal), whereas at the other temperatures they show a continuous decrease in shrinkage rate, as expected. The total isothermal shrinkage (with reference to the initial length of the specimen) at the various temperatures is reported in Fig. 3 (mean values of three measurements, the scatter being 0.03%).

Fig. 3. Isothermal shrinkage (60 min holding) as a function of temperature

The figure shows two discontinuities corresponding to T_C and the alpha/gamma transformation temperature. In both specimens, the isothermal shrinkage increases with temperature in the three temperature ranges, but it shows a sharp decrease passing through both the magnetic and allotropic transformations. Whereas the decrease from the alpha to the gamma field is attributed to the smaller self-diffusion coefficient of iron in the fcc lattice than in the bcc lattice, the decrease from the ferromagnetic to the paramagnetic bcc iron must be attributed to the different influence of the structuraldefects on bulk diffusivity. It is well-known that the effect of dislocation on bulk diffusivity, through the dislocation pipe diffusion mechanism, is significantly enhanced when approaching the Curie transformation.[21] Therefore, the results confirm the role of dislocations (both the pre-existing ones due to cold compaction and those generated by the structural changes in the neck regions) on the shrinkage kinetics. Figure 3 also shows the influence of temperature on the anisotropy of dimensional change; anisotropy is very pronounced below the Curie point [maximum ($\Delta l/l_{0,long}/\Delta l/l_{0,trans}$) = 2.1 at 730°C], decreases between T_C and Tα/γ [maximum ($\Delta l/l_{0,long}/\Delta l/l_{0,trans}$) = 1.5 at 860°C] and decreases further in austenite [maximum ($\Delta l/l_{0,long}/\Delta l/l_{0,trans}$) = 1.4 at 1060°C and 1120°C]. A shrinkage kinetic law accounting for the influence of prior cold compaction on the bulk diffusivity was proposed in,[14–16] introducing a time-dependent effective diffusion coefficient in the kinetic law of the classical theory of sintering.

The kinetic model is given by Eq. (1):

$$\frac{\Delta l}{l_0} = \left(\frac{80\ \ eff\gamma_s V_a}{2^5 kTD^3}\right)^{0.4} t^{0.4} \qquad (1)$$

where $\Delta l/l_0$ is the isothermal shrinkage, D_{eff} is the time-dependent effective volume diffusion coefficient, γ_s is the surface tension, V_a is the atomic volume, k is the Boltzmann constant, T is the absolute temperature, and D is the mean diameter of the powder particles. Equation (1) was used to calculate the effective volume diffusion coefficient from the isothermal shrinkage curves. Three examples are reported in Fig. 4, still representative of the other curves in the three temperature ranges: below the Curie point, in the alpha field above T_C, and in the austenite field.

Fig. 4. Examples of the effective diffusion coefficient versus isothermal holding time.

The curves show a different trend, depending on temperature. Below T_C, the effective diffusion coefficient increases up to a maximum and then decreases, whereas at the other two temperatures it increases continuously with a decreasing slope. The increase in bulk diffusivity is due to the continuous generation of dislocations in the growing neck region (structural activity), as proposed by Schatt and Friedrich,[24] until a critical dislocation density is reached that activates recovery and/or recrystallization. In this case, dislocation density begins to decrease, and diffusivity results are progressively attenuated. The observation of the maximum in the curves only below T_C demonstrates that the structural activity is much more pronounced in this temperature range than in the other two. From the curves shown in Fig. 4, the maximum effective diffusion coefficient (either the maximum or the highest value in the time range investigated) and the mean effective diffusion coefficient (weighted average) were calculated; they are reported in Fig. 5 versus temperature.

Fig. 5. Maximum and mean effective diffusion coefficient versus temperature

The figure shows that both the maximum and mean effective diffusivity increase with temperature within the three ranges considered, with a significant difference between the two directions in the alpha phase. The ratio between the two diffusivities along the transversal and longitudinal directions is shown in Fig. 6; here, the progressive enhancement of the anisotropy within the three ranges and its progressive attenuation moving from one range to the others are clearly shown.

Fig. 6. Ratio between the two diffusivities along the transversal and longitudinal directions

The effective diffusion coefficient is higher than the equilibrium coefficient—that is, the bulk diffusivity corresponding to an equilibrium density of structural defects that may be calculated from the activation energy data reported in the literature for pure iron.[27] The deviation from the reference values represents the enhancement of diffusivity due to the structural activity. Figure 7 shows the ratio of the maximum and mean effective diffusion coefficients to the reference coefficient along the two directions.

Fig. 7. $D_{eff\ max}/D_{eq}$ and $D_{eff\ mean}/D_{eq}$ versus temperature along the two directions

The structural activity is particularly intense below the Curie point and is much higher along the longitudinal direction than the transversal direction (diffusivity is enhanced by four orders of magnitude). At higher temperatures, it is much lower (maximum enhancement of diffusivity by two orders of magnitude) but is still higher along the longitudinal direction. It is small in the alpha field and increases when moving into the austenite field, where it decreases continuously with increasing temperature. The results of dilatometric tests

allow the conclusion that anisotropy of shrinkage in uniaxially cold compacted pure iron is due to the different structural activity of the material along the longitudinal and transversal directions, which results in a different effective bulk diffusivity. This conclusion and all data relevant to diffusivity come from the elaboration of the isothermal shrinkage curves modifying the shrinkage kinetic model given by Eq. (1), which was proposed assuming rigid spherical particles in a point contact at the beginning of the sintering process. This model does not consider plastic deformation caused by cold compaction, which:

1. Introduces a high density of structural defects, mainly dislocations, in the contact regions;
2. Forms an area contact between the particles.

The structural and geometrical conditions of the particles in the green compact are therefore quite different from that assumed in the sintering theory. With regard to the effect on sintering, the structural defectiveness and the large contact area have a strong interaction that influences the mass transport mechanism responsible for neck growth. The contact area is the source of atoms diffusing toward the neck surface; therefore, the flux of atoms is greater than that in the case of an initial point contact. Because the self-activated sintering mechanism proposed by Schatt and Friedrich is caused by the dislocations produced by the transformation of the contact area in a grain boundary, the existence of a "large" contact area instead of a point contact is expected to enhance sintering directly (owing to the larger source of atoms) and indirectly (owing to the generation of a larger density of dislocations). Moreover, dislocations introduced by cold compaction enhance diffusion and, in turn, the transformation of the contact surface in a grain boundary; they are therefore expected to enhance the self-activation of sintering. The combined effect of these phenomena is that of enhancing diffusivity in the neck region significantly, which may be reasonably contemplated in the kinetic model by means of the effective diffusion coefficient considered here. Under this assumption, the anisotropy of shrinkage finds a coherent interpretation, considering that the powder particles are inhomogeneously deformed by the uneven distribution of pressure during uniaxial compaction, as demonstrated by the SEM image of the green specimens used in the present work (the compaction is in the vertical direction) shown in Fig. 8.

Fig. 8. SEM micrograph of the green parts.

As a result, both dislocation density and the starting extension of the contact area in the interparticle contact regions perpendicular to the compaction direction are higher than those in the directions parallel to it. This will result in a marked anisotropy of both the structural (related to deformation) and geometrical (related to extension of the contact regions) activity of the material, thus making the shrinkage kinetics faster along the longitudinal direction than those along the transversal direction. This effect is very pronounced in the early stage of sintering below T_C, where the structural defectiveness has the biggest effect on diffusivity and decreases at higher temperatures. In the alpha field, the effect of prior cold compaction on the structural defectiveness is still present, whereas in austenite, most defects introduced by cold compaction should be eliminated by recrystallization accompanying the phase transformation. As a consequence, anisotropy in the

austenite region is expected to be due to the different geometrical activity only. The resolution of the two contributions and the introduction of a parameter accounting for geometrical activity in the shrinkage kinetic model are matters of further work.

Coming back to the effective diffusion coefficient, curves similar to those in Fig. 4 may be fitted by Eq. (2):

$$D_{eff} = \frac{t}{a+bt-ct^{0.97}} \qquad (2)$$

as shown in Fig. 9. The dependence on temperature of parameters a, b, and c is shown in Fig. 10.

Fig. 9. Experimental and fit curves of the effective diffusion coefficient

Fig. 10. Constants a, b, and c of Eq. (2) versus temperature.

Equation (2) does not have a physical meaning related to the phenomena responsible for the initial increase and the possible decrease in the effective diffusion coefficient (continuous generation of dislocations and recovery/recrystallization). The theory of the dislocation pipe diffusion proposes a linear correlation between volume diffusion and dislocation density. Therefore, the dependence of the effective diffusion coefficient on time should result from the combination of the square root dependence proposed by Schatt and Friedrich for the increase in the dislocation density in the neck region and the logarithmic dependence proposed for the decrease due to recovery and recrystallization, considering that recovery/recrystallization begin only after a given dislocation density has been reached. Any attempt to implement such a physical model valid in the three considered temperature ranges has failed, whereas Eq. (2) fits experimental data quite well at all temperatures investigated. With the exception of the data relevant to the lowest temperature, Fig. 8 highlights a linear correlation in the three temperature ranges, so that the model of the effective diffusion coefficient may be completed by the following equations:

$$loga = m_a T + q_a \qquad (3)$$

$$logb = m_b T + q_b \qquad (4)$$

$$logc = m_c T + q_c \qquad (5)$$

where T is in °C and m_b and q_b are very similar to m_c and q_c, respectively. Equation (2) may therefore be rewritten as

$$D_{eff} = \frac{t}{a+b(t-t^{0.97})} \qquad (6)$$

with parameters m and q listed in Table I.

Table I. Parameters of Eqs. (3)–(5)

The elaboration of shrinkage curves does not consider the different extension of the contact areas along the directions parallel and perpendicular to the compaction direction, which is also expected to have an important effect on anisotropy. Indeed, the contact area between the deformed particles is the source of atoms diffusing toward the neck; the larger its extension, the more intense are the flux of atoms. The

contribution of this geometrical characteristic to anisotropy of shrinkage is expected to dominate that given by dislocations in austenite because strain hardening promoted by cold compaction should be mostly eliminated by the alpha/gamma phase transformation. Work is in progress to investigate this contribution, which requires a reliable measure of the extension of the contact areas.

IV. Conclusions

The anisotropy of sintering shrinkage of a 6.9 g/cm^3 green density iron was investigated by dilatometry in the range 640°C–1120°C with 1 h of isothermal holding. Anisotropy is very pronounced below the Curie temperature [maximum ($\Delta l/l_{0,long}/\Delta l/l_{0,trans}$) = 2.1 at 730°C], decreases between T_C and Tα/γ [maximum ($\Delta l/l_{0,long}/\Delta l/l_{0,trans}$) = 1.5 at 860°C] and decreases further in austenite [maximum ($\Delta l/l_{0,long}/\Delta l/l_{0,trans}$) = 1.4 at 1060°C and 1120°C]. The isothermal shrinkage curves were elaborated using the shrinkage kinetic equation proposed by the sintering theory, introducing an effective diffusion coefficient, which accounts for all deviations of the uniaxially cold compacted material from the model of rigid spheres. Such an effective diffusion coefficient is higher along the longitudinal direction than along the transversal direction (the ratio between the longitudinal and transversal effective coefficients is up to 10 below the Curie point, 2.5 above T_C in the alpha field and 1.3 in the austenite field), and it is also higher than the bulk diffusivity of iron in the presence of an equilibrium density of dislocations (up to four orders of magnitude below the Curie point). This is expected because the powder particles are heavily plastically deformed after uniaxial cold compaction, and dislocations enhance bulk diffusivity through the dislocation pipe diffusion mechanism. The effective diffusion coefficient increases with time, and below the Curie temperature, it reaches a maximum and decreases. In addition to the pre-existing dislocations, others are generated during neck growth according to the self-activation theory of sintering; a critical dislocation density may be reached that activates recovery/recrystallization (decrease). The maximum is observed only below the Curie transformation, where the effect of dislocations on bulk diffusivity is particularly pronounced. Anisotropy of shrinkage may therefore be justified by the inhomogeneous deformation of the powder particles due to the uneven distribution of pressure along the compaction direction and perpendicular to it during uniaxial cold compaction. An equation correlating the effective diffusion coefficient to time and temperature was proposed.

References

1 I. Cristofolini, C. Menapace, M. Cazzolli, A. Rao, W. Pahl, and A. Molinari, “The Effect of Anisotropic Dimensional Change on the Precision of Steel Parts Produced by Powder Metallurgy,” J. Mater. Process. Technol., 212, 1513–9 (2012).

2 I. Cristofolini, M. Pilla, M. Larsson, and A. Molinari, “A DOE Analysis of Dimensional Change on Sintering of a 3%Cr-0.5%Mo-x%C Steel and Its Effect on Dimensional and Geometrical Precision,” Powder Metall. Prog., 3 [12] 127–43 (2012).

3 I. Cristofolini, M. Pilla, A. Rao, S. Libardi, and A. Molinari, “Dimensional and Geometrical Precision of Powder Metallurgy Parts Sintered and Sinterhardened at High Temperature,” Int. J. Precis. Eng. Man., 14 [10] 1735–42 (2013).
4 I. Cristofolini, A. Molinari, M. Pilla, C. Menapace, and M. Larsson, “A DOE Investigation on Anisotropic Dimensional Change on Fe-C-Cu Sintering,” Int. J. Powder Metall., 48 [4] 33–43 (2012).
5 I. Cristofolini, N. Corsentino, M. Pilla, A. Molinari, and M. Larsson, “Influence of Geometry on the Anisotropic Dimensional Change on Sintering of PM Parts”; pp. 49–61 in Adv PM Part, Vol. 1, Edited by D. Christophersson and R. M. Gavior. Metal Powder Industries Federation, Princeton, NJ, 2013.
6 E. A. Olevsky, “Theory of Sintering: From Discrete to Continuum,” Mater. Sci. Eng., R, 23, 41–100 (1998).
7 F. Wakai, K. Chihara, and M. Yoshida, “Anisotropic Shrinkage Induced by Particle Rearrangement in Sintering,” Acta Mater., 55, 4553–66 (2007).
8 F. Wakai and Y. Shinoda, “Anisotropic Sintering Stress for Sintering of Particles Arranged in Orthotropic Symmetry,” Acta Mater., 57, 3955–64 (2009).
9 F. Wakai and T. Akatsu, “Anistropic Viscosities and Shrinkage Rate in Sintering of Particles Arranged in Simple Orthorhombic Structure,” Acta Mater., 58, 1921–9 (2010).
10 E. A. Olevsky and R. M. German, “Effect of Gravity on Dimensional Change During Sintering – I. Shrinkage Anisotropy,” Acta Mater., 48, 1153–66 (2000).
11 R. K. Bordia, R. Zuo, O. Guillon, S. M. Salamone, and J. R€odel, “Anisotropic Constitutive Laws for Sintering Bodies,” Acta Mater., 54, 111–8 (2006).
12 A. Zavaliangos and D. Bouvard, “Numerical Simulation of Anisotropy in Sintering Due to Prior Compaction,” Int. J. Powder Metall., 36 [7] 59–65 (2000).
13 A. Zavaliangos, J. M. Missiaen, and D. Bouvard, “Anisotropy in Shrinkage During Sintering,” Sci. Sinter., 38, 13–25 (2006).
14. Molinari, E. Bisoffi, C. Menapace, and J. M. Tollalba, “Shrinkage Kinetics During the Early Stage of Sintering: The Time Depending Effective Diffusion Coefficient”; pp. 285–90 in Proceedings EuroPM2013 Congress & Exhibition, Vol. 2, Ed. EPMA, Shrewsbury, UK, 2013.
15 A. Molinari, E. Bisoffi, C. Menapace, and J. Torralba, “Shrinkage Kinetics During Early Stage Sintering of Cold Isostatically Compacted Iron Powder,” Powder Metall., 57 [1] 61–9 (2014).
16 A. Molinari, C. Menapace, E. Torresani, I. Cristofolini, and M. Larsson, “Working Hypothesis for Origin of Anisotropic Sintering Shrinkage Caused by Prior Uniaxial Cold Compaction,” Powder Metall., 56 [3] 189–95 (2013).
17 A. Molinari, E. Torresani, C. Menapace, I. Cristofolini, and M. Larsson, “A Study of Sintering Shrinkage Kinetics of Cold Compacted Ferrous Green Parts”; pp. 25–32 in Adv PM Part, Vol. 5, Edited by D. Christophersson and R. M. Gavior. Metal Powder Industries Federation, Princeton, NJ, 2013.
18 L. Emanuelli, C. Menapace, I. Cristofolini, A. Molinari, and M. Larsson, “Influence of Sintering Temperature on Shrinkage Anisotropy in Cr-Mo Low Alloy Steel Green Compacts”; pp. 99–107 in Adv PM

Part, Vol. 1, Edited by R. A. Chernenkoff and W. Brian James. Metal Powder Industries Federation, Princeton, NJ, 2014.
19 N. Corsentino, C. Menapace, I. Cristofolini, M. Pilla, M. Larsson, and A. Molinari, "A Dilatometry Study of the Influence of the Liquid Phase on Anisotropy of Dimensional Change of Iron Alloys," Int. J. Powder Metall., 51 [2], 13–21 (2014).
20 P. Shewmon, Diffusion in Solids, Second edition, pp. 202–5. The Minerals, Metals and Materials Society, Warrendale, PA, 1989.
21 Y. Shima, et al., "Self-Diffusion Along Dislocations in Ultra High Purity Iron," Mater. Trans., 43 [2] 173–7 (2002).
22 E. Friedrich and W. Schatt, "Sintering of one-Component Model Systems: Nucleation and Movement of Dislocations in Necks," Powder Metall., 4, 193–7 (1980).
23 E. Friedrich and W. Schatt, "Spannungsverteilung und Versetzungsvervielfachung in der Sinterkontaktregion," Acta Metall., 31, 121–8 (1983).
24 E. Friedrich and W. Schatt, "High Temperature Plasticity in Solid Phase Sintering," Sci. Sinter., 5, 63–71 (1983).
25 W. Schatt, B. Vetter, and E. Friedrich, "Non- Isothermal Shrinkage of Compacts," Powder Metall., 34 [3] 179–82 (1991).
26 P. Lanyi and W. Hermel, "Structural Activity and Shrinkage Kinetics in Early Stages of Sintering Process," Powder Metall., 2, 93–100 (1981).
27 C. J. Smithells, Smithells Metals Reference Book, chapter 13.3. Edited by E. A. Brandes. Buttherworths, London, 1983.

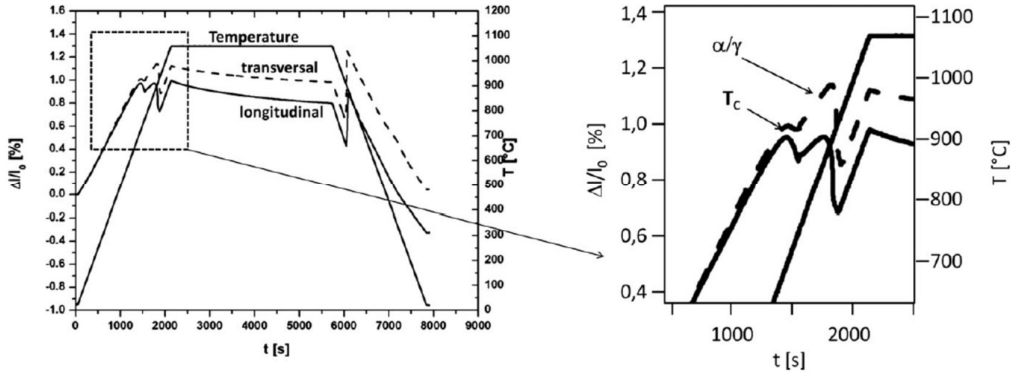

Figure 1

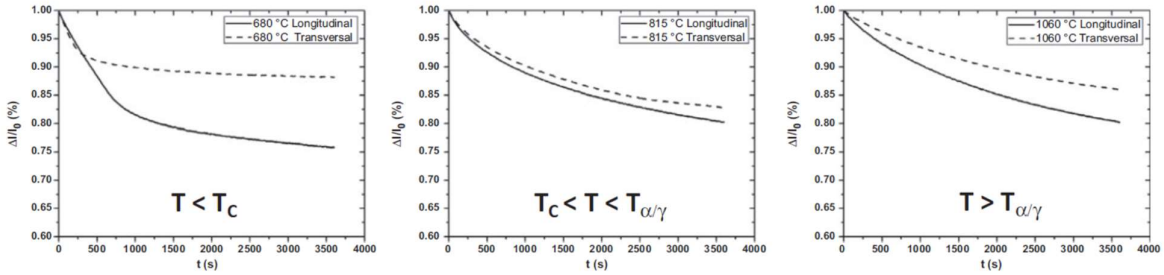

Figure 2

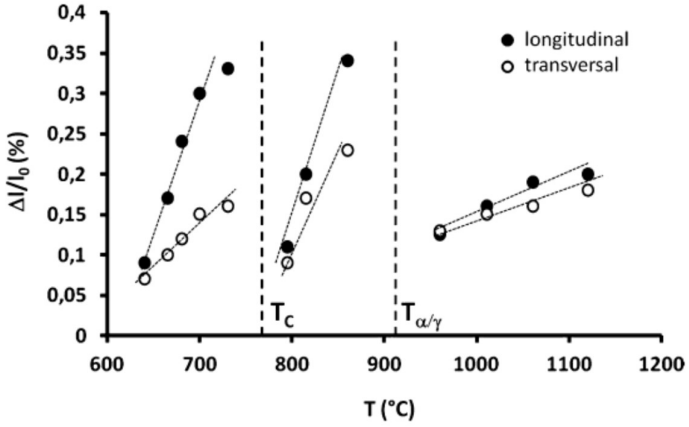

Figure 3

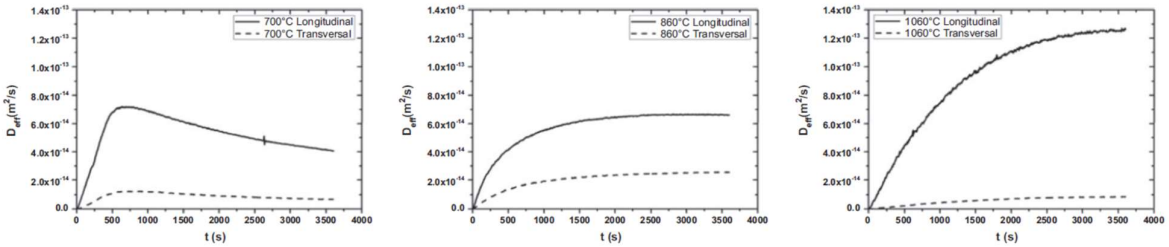

Figure 4

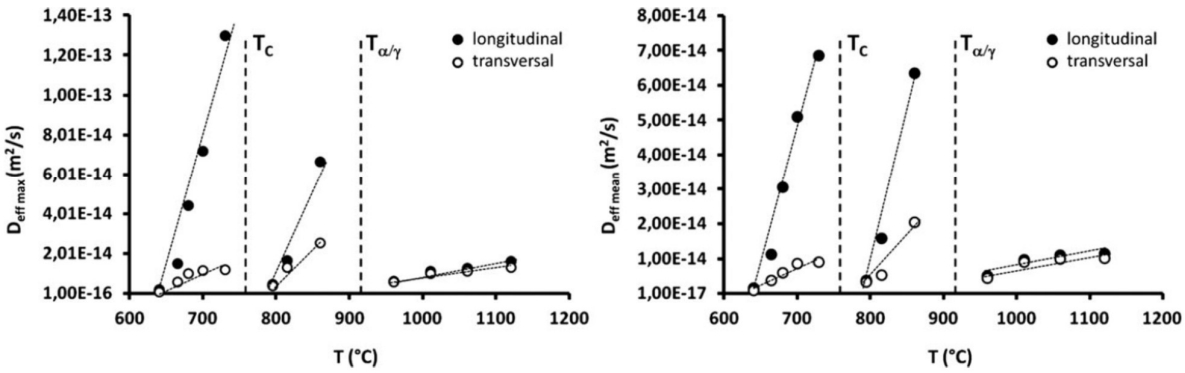

Figure 5

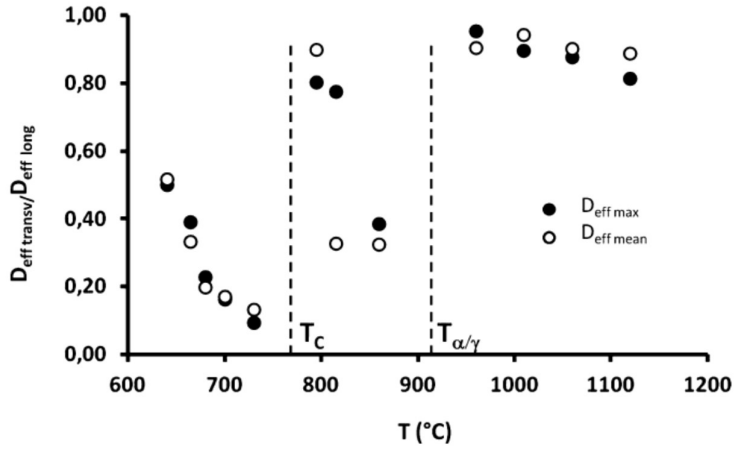

Figure 6

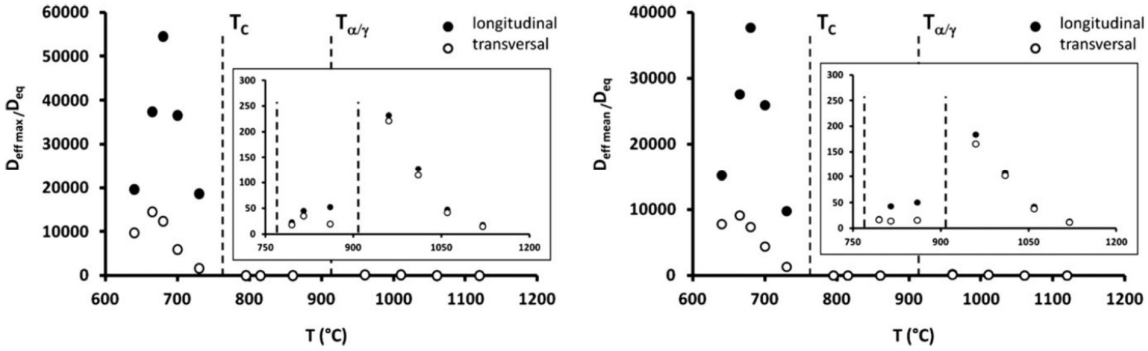

Figure 7

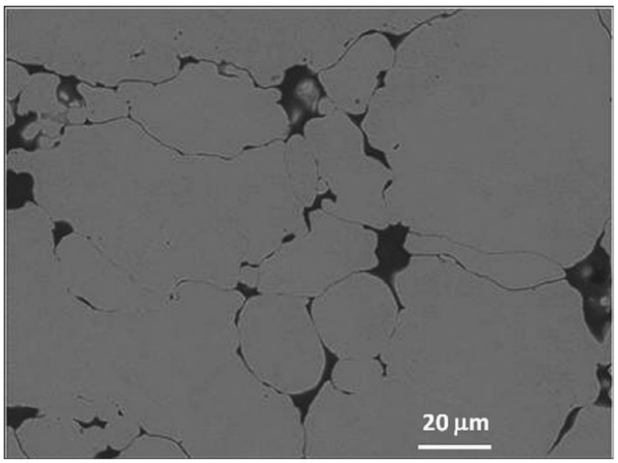

Figure 8

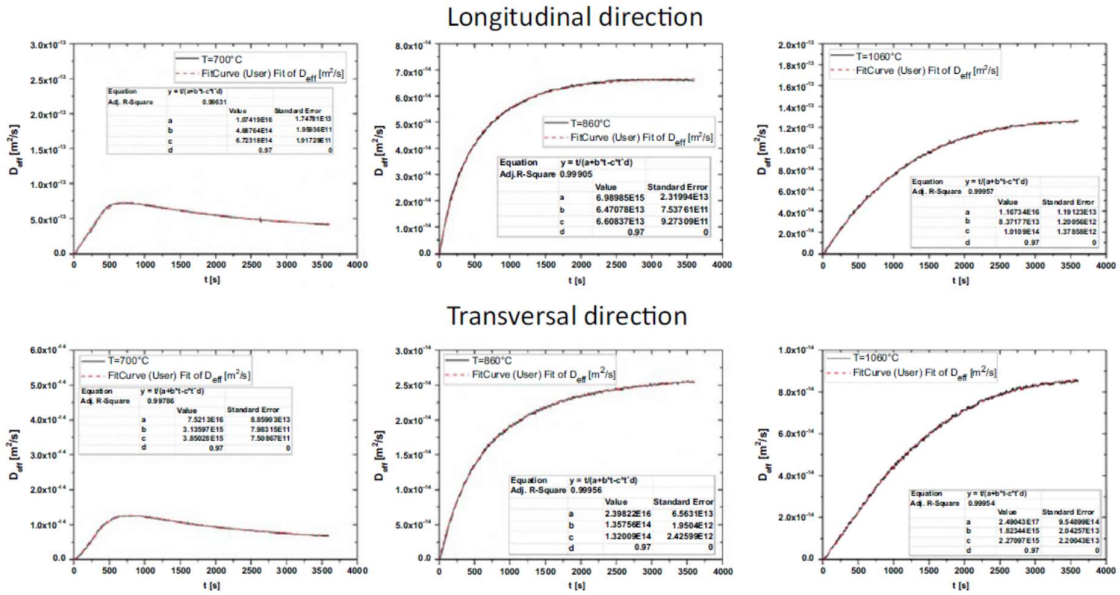

Figure 9

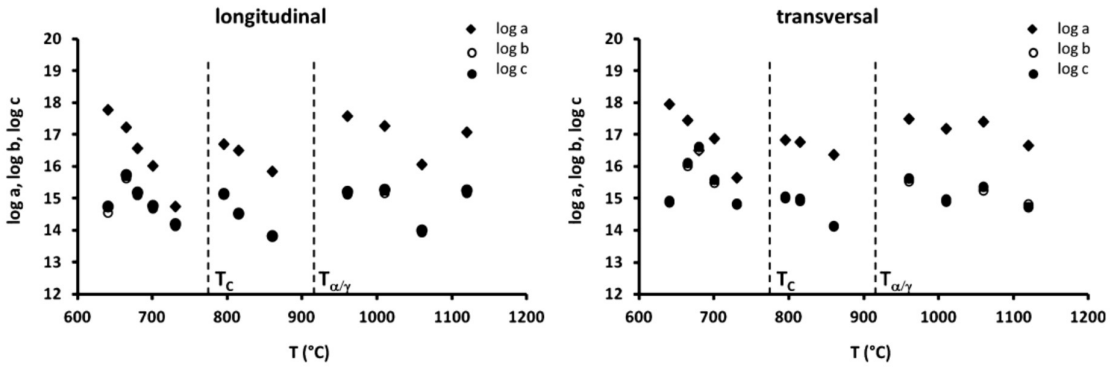

Figure 10

Tab. I

Parameter	660°C < T < T_C		T_C < T < Tα/γ		Tα/γ < T < 1120°C	
	Longitudinal	Transversal	Longitudinal	Transversal	Longitudinal	Transversal
m_a	-0.034	-0.024	-0.013	-0.007	-0.005	-0.005
q_a	39.6	33.7	27.4	22.6	22.0	22.0
$m_b = m_c$	-0.022	-0.019	-0.020	-0.014	-0.002	-0.003
$q_b = q_c$	30.5	29.1	30.5	26.3	16.8	18.7